Journal of Sound and Vibration 558 (2023) 117759

Contents lists available at ScienceDirect

Journal of Sound and Vibration

journal homepage: www.elsevier.com/locate/jsvi

Modeling and efficiency maximization of magnetostrictive energy harvester under free vibration

Yoshito Mizukawa *, Umair Ahmed, David Blažević, Paavo Rasilo

Tampere University, Electrical Engineering, Korkeakoulunkatu 3, Tampere, Finland

ARTICLE INFO

Keywords:
Efficiency maximization
Energy harvesting
Free vibration
Linearized modeling
Magnetostriction
Primary damping

ABSTRACT

Vibration energy harvesting is becoming increasingly attractive in line with the development of wireless sensor technologies. Magnetostrictive materials inherently exhibit high mechanical strength and are thus suitable for various applications and mass manufacturing of energy harvesting devices. Many studies have been conducted to increase the output power of harvesters, and some utilized analytical methods. However, the optimization methods often take into account only the resonant frequency of the system under forced vibration. These models can produce correct predictions only when steady-state harmonic excitation inputs are considered.

In this study, we propose the modeling and optimization method for a cantilever-type magnetostrictive harvester under free vibration. The cantilever has a double-beam structure composed of two parallel Fe-Ga beams with pickup coils. In the modeling, the shape function of the cantilever-type magnetostrictive energy harvester was derived based on the continuity of the internal force and magnetic flux. Hamilton's principle for an electromagnetic-mechanically coupled system was derived from the virtual work principle. The equation of motion, magnetic circuit equation, and electric circuit equation of the system were respectively derived from the corresponding Euler–Lagrange equations. The harvestable energy of the magnetostrictive energy harvester was calculated by using the symmetric property of eigenvalues. In the efficiency maximization of the harvestable energy, we found that the optimal solution differs depending on the type of given energy. The optimal parameters to maximize the energy efficiency to potential energy and kinetic energy are respectively derived in the form of algebraic solutions. Experimental validation was conducted by measuring the energy harvesting efficiency at different loads.

1. Introduction

Vibration energy harvesting has gained attention in the last two decades in line with the growing popularity of wireless sensor networks [1] and Internet of Things applications [2]. To convert the energy of mechanical vibrations to electrical energy, electromagnetic and piezoelectric transducers have been commonly researched and used in various applications [3]. Anton et al. [4] performed an experimental proof of concept of vibration energy harvesting in aircraft with an aircraft model. They attached piezoelectric patches to the wing spar and installed a cantilever-type piezoelectric energy harvester into the fuselage of the aircraft. The harvested energy was sufficient for powering low-power subsystems. Tang et al. [5] installed an electromagnetic energy harvester at the top of a prototype building as a damper. The harvested energy was used to actively control the damping. They

* Corresponding author.
E-mail address: yoshito.mizukawa@tuni.fi (Y. Mizukawa).

https://doi.org/10.1016/j.jsv.2023.117759
Received 10 January 2023; Received in revised form 26 April 2023; Accepted 28 April 2023
Available online 6 May 2023

validated the effectiveness of the self-powered active vibration suppression using an energy harvester. Yoshida et al. [6] conducted on-site experiments with piezoelectric energy harvesters for structural health monitoring of railway bridges. The harvested energy was supplied to the sensor systems attached to the railway bridge and in this way, a whole wireless structural monitoring system for railway bridges was established.

Electromagnetic energy harvesting utilizes the electromotive force induced by the change of magnetic flux. Beeby et al. [7] presented an electromagnetic micro harvester consisting of a cantilever with a wound coil and magnets. The device produced 46 μW with practical volume of 0.15 cm^3 under 0.59 m s^{-2} acceleration at its resonant frequency of 52 Hz. Abohamer et al. [8,9] proposed the development of pendulum-type electromagnetic energy harvesters where they analyzed the non-linear behaviors and stabilities of the harvesters by employing the method of multiple scales. Zuo et al. [10] proposed electromagnetic energy harvesting tuned mass dampers where they maximized the output power based on the H_2 norm with the assumption that the system is excited by white noise input.

Piezoelectric energy harvesters are characterized by their high energy density and simple device structure. Erturk and Inman [11] analyzed a cantilevered piezoelectric harvester by modal decomposition. They also investigated the effect of tip mass and proved that the error of the single-degree-of-freedom modeling method decreases as the mass ratio of the tip mass to the beam increases. Lefeuvre et al. [12] analyzed an RC circuit coupled to a single-degree-of-freedom mechanical system. They maximized the average power of the load resistance and proved that the dc–dc buck–boost converter can be modeled as a resistor for fixed values of the duty cycle and the switching frequency. However, piezoelectric materials cannot be used in applications involving strong mechanical force due to their brittleness [13]. In addition, the most common piezoelectric material, perovskite lead zirconate titanate, contains lead and its high toxicity has been a great concern [14,15].

Magnetostrictive energy harvesting utilizes magnetic induction based on Joule and Villari effects present in giant magnetostrictive materials to convert between strain energy and magnetic energy. Palumbo et al. [16] investigated the change of magnetostrictive properties of a Fe-Ga energy harvester under different mechanical prestress and magnetic bias. The optimal values of these parameters are discussed based on the experiments. Ahmed et al. [17–19] conducted finite element analyses of magnetostrictive energy harvesters based on the Helmholtz free energy density function. Mizukawa et al. [20] analytically investigated the magnetostrictive energy harvester and derived its optimal resistance and optimal capacitance as functions of the excitation frequency. Ueno and Yamada [21] proposed a cantilever-type micro energy harvesting device consisting of two parallel Fe-Ga beams. They experimentally investigated the energy harvesting efficiency of the proposed device and demonstrated that the energy harvesting efficiency is linear with respect to initial displacement. Wang and Yuan [22] analyzed a cantilever-type magnetostrictive harvester using Metglas bonded on a copper substrate. They applied Hamilton's principle in the magneto-mechanical part of the system to obtain the equation of motion. They assumed an infinitely long solenoid coil and thus neglected the effect of the magnetic circuit.

Although many studies have been conducted to increase the energy efficiency of energy harvesters, most of them have focused on the resonant state of the harvesters under forced vibration. While the resonance-based approach is effective when harmonic excitation is given to the system, it cannot be applied to the system oscillating without external force. When harvesters are used in applications involving random impacts, they have to be optimized based on free vibration. In this paper, we propose a modeling and optimization method for a magnetostrictive energy harvester under free vibration. In the modeling process, we assumed that the deflection of the harvester due to shear stress was negligibly small compared to the bending deflection [23] and that the vibration amplitude of the harvester was sufficiently small. Therefore, the linearized approach and the Euler–Bernoulli beam theory were used [22,24–26]. The equation of motion, magnetic circuit equation, and electric circuit equation of the harvester are obtained from the Euler–Lagrange equations derived based on the virtual work principle. Energy harvesting efficiency and efficiency-maximizing design parameter were derived depending on whether the free vibration is induced by initial displacement or initial velocity. The efficiency calculations are validated through experiments.

2. Modeling method

In this study, we analyze the double-beam magnetostrictive energy harvester proposed in [21]. The harvester consists of two parallel Fe-Ga beams. The coils wound around the Fe-Ga beams are connected in series with a load resistor. Permanent magnets are attached to the ends of the double beam to give symmetric magnetic bias to the Fe-Ga beams. The magnetic flux flowing into the magnets and air is static, and thus negligible in the linear dynamics. Fig. 1 shows the (a) side view and (b) top view of the double-beam magnetostrictive energy harvester connected to a resistive circuit.

2.1. Constitutive equations

The magnetostrictive constitutive equations linearized for small-signal behavior are given as follows [25]:

$$\begin{aligned} \Delta \boldsymbol{B} &= \left[\mu^{\mathrm{T}}\right] \Delta \boldsymbol{H} + [d]^{*} \Delta \boldsymbol{T} \\ \Delta \boldsymbol{S} &= [d] \Delta \boldsymbol{H} + \left[s^{\mathrm{H}}\right] \Delta \boldsymbol{T} \end{aligned} \tag{1}$$

where $\boldsymbol{B}$, $\boldsymbol{H}$, $\boldsymbol{S}$, and $\boldsymbol{T}$ are the magnetic flux density, magnetic field strength, mechanical strain, and mechanical stress, respectively. The small variation of the quantities is denoted by Δ. $\left[\mu^{\mathrm{T}}\right]$ is the permeability matrix at constant stress, $\left[s^{\mathrm{H}}\right]$ is the elastic compliance

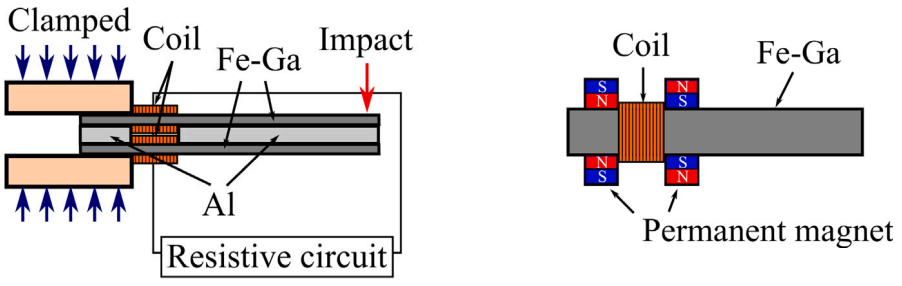

(a) Side view (b) Top view

Fig. 1. Double-beam magnetostrictive energy harvester connected to a resistive circuit.

matrix at constant magnetic strength, $[d]^*$ is the transpose of the magnetostrictive constant matrix $[d]$. In this study, we consider only the longitudinal direction, and thus Eqs. (1) can be represented as 1D constitutive equations:

$$\begin{bmatrix} \Delta B \\ \Delta S \end{bmatrix} = \begin{bmatrix} \mu^{\mathrm{T}} & d \\ d & s^{\mathrm{H}} \end{bmatrix} \begin{bmatrix} \Delta H \\ \Delta T \end{bmatrix} \tag{2}$$

By multiplying the inverse of the coefficient matrix from the left, we can solve Eq. (2) with regards to ΔH and ΔT:

$$\begin{bmatrix} \Delta H \\ \Delta T \end{bmatrix} = \begin{bmatrix} \dfrac{\nu^{\mathrm{T}}}{1-k_0^2} & -\dfrac{\nu^{\mathrm{T}} E^{\mathrm{H}} d}{1-k_0^2} \\ -\dfrac{\nu^{\mathrm{T}} E^{\mathrm{H}} d}{1-k_0^2} & \dfrac{E^{\mathrm{H}}}{1-k_0^2} \end{bmatrix} \begin{bmatrix} \Delta B \\ \Delta S \end{bmatrix} \tag{3}$$

where $\nu^{\mathrm{T}} = 1/\mu^{\mathrm{T}}$ and $E^{\mathrm{H}} = 1/s^{\mathrm{H}}$ are the reluctivity and Young's modulus. The magnetostrictive coupling coefficient k_0 is defined as follows:

$$k_0 = \frac{d}{\sqrt{\mu^{\mathrm{T}} s^{\mathrm{H}}}} \tag{4}$$

2.2. Derivation of shape function

The shape function of the cantilever is generally derived by solving the Euler–Bernoulli beam equation and frequency equation. This section demonstrates that the shape function of the double-beam cantilever can be obtained in a simple way by considering the continuity of the internal force and magnetic flux.

Fig. 2 shows the configuration of the double beam subject to bending. Assuming that the cantilever oscillates with only its fundamental mode of oscillation, the displacement $W_{(x,t)}$ is expressed as a product of a function of longitudinal coordinate x and a function of time t:

$$W_{(x,t)} = \psi_{(x)} \eta_{(t)} \tag{5}$$

where $\psi_{(x)}$ and $\eta_{(t)}$ are the shape function and generalized displacement, respectively. From the Euler–Bernoulli beam assumption, the strain ΔS is represented as follows:

$$\Delta S = -z \frac{\partial^2 W_{(x,t)}}{\partial x^2} = -z \frac{\partial^2 \psi_{(x)}}{\partial x^2} \eta_{(t)} \tag{6}$$

where z is the distance from the neutral plane. Similarly, the magnetic flux density ΔB is assumed to be linear with respect to z:

$$\Delta B = \frac{z}{z_0} B_{\mathrm{ave}(t)} \tag{7}$$

where z_0 is the distance from the neutral plane to the upper Fe-Ga beam. $B_{\mathrm{ave}(t)}$ is the average magnetic flux density which satisfies the continuity of the magnetic flux. It results from the continuity of the internal force that the surface integral of the mechanical stress ΔT of Eq. (3) over the cross-sectional area A,

$$\int_A \Delta T \mathrm{d}A = -\int_A \frac{z}{z_0} \mathrm{d}A \frac{\nu^{\mathrm{T}} E^{\mathrm{H}} d}{1-k_0^2} B_{\mathrm{ave}(t)} - \int_A z \mathrm{d}A \frac{E^{\mathrm{H}}}{1-k_0^2} \frac{\partial^2 \psi_{(x)}}{\partial x^2} \eta_{(t)} \tag{8}$$

must be independent of the longitudinal coordinate x. Thus, $\dfrac{\mathrm{d}^2 \psi_{(x)}}{\mathrm{d}x^2}$ is constant and the stress becomes

$$\Delta S = -z \frac{\partial^2 \psi_{(x)}}{\partial x^2} \eta_{(t)} = -zC\eta_{(t)} \tag{9}$$

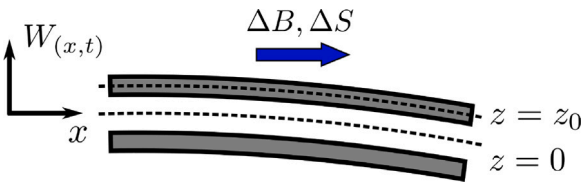

Fig. 2. Configuration of the double beam subject to bending.

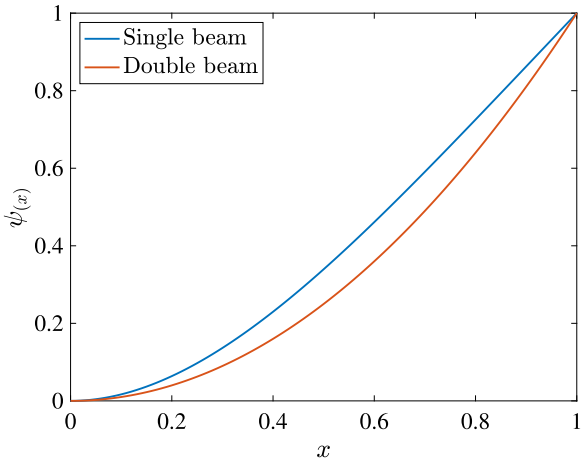

Fig. 3. Comparison of shape functions between single beam and double beam.

where C is a constant. With consideration of the boundary conditions for the cantilever,

$$\psi_{(0)} = 0, \qquad \psi'_{(0)} = 0 \tag{10}$$

the shape function $\psi_{(x)}$ is obtained as follows:

$$\psi_{(x)} = \frac{1}{2} C x^2 \tag{11}$$

Fig. 3 compares the derived shape function Eq. (11) for the double beam with the fundamental shape function of a single beam derived by solving the Euler–Bernoulli beam equation and frequency equation. Each shape function is normalized to be 1 at $x = 1$. The derived shape function has a greater curvature than the fundamental shape function for a single beam.

2.3. Hamilton's principle for electromagnetic-mechanical coupled system

In this section, we derive Hamilton's principle for the electromagnetic-mechanical conserved system based on the virtual work principle. For the mechanical system, the virtual work principle is applied to D'Alembert's principle as

$$\delta V_{\mathrm{mec}} = (f - m\ddot{\eta})\,\delta\eta \tag{12}$$

where V_{mec} is the virtual work done by the mechanical system, f and m are the generalized force and generalized mass, respectively, and δ denotes the infinitesimally small arbitrary quantity. The first term in Eq. (12) can be represented with the potential energy U as

$$f\,\delta\eta = -\delta U \tag{13}$$

The second term in Eq. (12) can be represented as

$$-m\ddot{\eta}\delta\eta = m\dot{\eta}\delta\dot{\eta} - \frac{\mathrm{d}}{\mathrm{d}t}(m\dot{\eta}\delta\eta) = \delta K - \frac{\mathrm{d}}{\mathrm{d}t}(m\dot{\eta}\delta\eta) \tag{14}$$

where K is the kinetic energy. With Eqs. (13) and (14), Eq. (12) becomes

$$\delta V_{\mathrm{mec}} = \delta K - \delta U - \frac{\mathrm{d}}{\mathrm{d}t}(m\dot{\eta}\delta\eta) \tag{15}$$

For the electric and magnetic systems, the virtual work principle is applied to Kirchhoff's second law in the electric and magnetic circuits, respectively:

$$\begin{aligned}\delta V_{\mathrm{ele}} &= \left(e_{\mathrm{EMF}} - e\right)\delta q \\ \delta V_{\mathrm{mag}} &= \left(F_{\mathrm{MMF}} - F\right)\delta\phi\end{aligned} \tag{16}$$

where V_{ele} and V_{mag}, respectively, are the virtual works done by electric and magnetic systems. e_{EMF} and F_{MMF} are the electromotive and magnetomotive forces, respectively. e and F are the electric and magnetic potential differences of the circuit components, respectively. q and ϕ are the electric charge and magnetic flux, respectively. The first terms on the right-hand sides of Eqs. (16) can be represented by Faraday's and Ampere's laws as

$$\begin{aligned}e_{\mathrm{EMF}}\delta q &= -N\dot{\phi}\delta q = N\phi\delta\dot{q} - \frac{\mathrm{d}}{\mathrm{d}t}\left(N\phi\delta q\right) \\ F_{\mathrm{MMF}}\delta\phi &= N\dot{q}\delta\phi\end{aligned} \tag{17}$$

where N is the number of turns in the coil. The second terms in Eqs. (16) can be represented as

$$\begin{aligned}-e\delta q &= \delta K_{\mathrm{e}} - \delta U_{\mathrm{e}} - \frac{\mathrm{d}}{\mathrm{d}t}\left(L\dot{q}\delta q\right) \\ -F\delta\phi &= -\delta U_{\mathrm{m}}\end{aligned} \tag{18}$$

where K_{e}, U_{e} and U_{m} are the energy of the coil with inductance L, the energy of the capacitor and magnetic field energy, respectively. From Eqs. (15)–(18), the virtual work principle for the electromagnetic-mechanical conserved system can be obtained as

$$\begin{aligned}&\delta V_{\mathrm{mec}} + \delta V_{\mathrm{ele}} + \delta V_{\mathrm{mag}} = \left(f - m\ddot{\eta}\right)\delta\eta + \left(F_{\mathrm{MMF}} - F\right)\delta\phi + \left(e_{\mathrm{EMF}} - e\right)\delta q \\ &= \delta\left(K + K_{\mathrm{e}} + N\phi\dot{q} - U - U_{\mathrm{e}} - U_{\mathrm{m}}\right) - \frac{\mathrm{d}}{\mathrm{d}t}\left(m\dot{\eta}\delta\eta + L\dot{q}\delta q + N\phi\delta q\right) = 0\end{aligned} \tag{19}$$

where

$$\delta\left(N\phi\dot{q}\right) = N\left(\phi + \delta\phi\right)\left(\dot{q} + \delta\dot{q}\right) - N\phi\dot{q} \tag{20}$$

By integrating Eq. (19) between arbitrary time instants ($t \in [t_{\mathrm{a}}, t_{\mathrm{b}}]$), the following equation can be obtained:

$$\int_{t_{\mathrm{a}}}^{t_{\mathrm{b}}} \delta\mathcal{L}\mathrm{d}t - \left[m\dot{\eta}\delta\eta + L\dot{q}\delta q + N\phi\delta q\right]_{t_a}^{t_b} = 0 \tag{21}$$

where $\mathcal{L}$ is the Lagrangian:

$$\mathcal{L} = K + K_{\mathrm{e}} + N\phi\dot{q} - U - U_{\mathrm{e}} - U_{\mathrm{m}} \tag{22}$$

For the cantilever-type magnetostrictive harvester shown in Fig. 1, each term in Eq. (22) is given by

$$\begin{aligned}K &= \frac{1}{2}m\dot{\eta}^2 = 2\int_0^l \frac{1}{2}\rho A\left(\psi_{(x)}\dot{\eta}\right)^2\mathrm{d}x + \frac{1}{2}m_{\mathrm{t}}\left(\psi_{(l)} + \frac{1}{2}\left.\frac{\partial\psi_{(x)}}{\partial x}\right|_{x=l} l_{\mathrm{t}}\right)^2\dot{\eta}^2 + \frac{1}{2}J_{\mathrm{t}}\left(\left.\frac{\partial\psi_{(x)}}{\partial x}\right|_{x=l}\dot{\eta}\right)^2 \\ K_{\mathrm{e}} &= \frac{1}{2}L\dot{q}^2 = 0 \\ U &= 2\int_0^l\int_A u\mathrm{d}A\mathrm{d}x \\ U_{\mathrm{e}} &= 0 \\ U_{\mathrm{m}} &= 2\int_0^l\int_A u_{\mathrm{m}}\mathrm{d}A\mathrm{d}x\end{aligned} \tag{23}$$

where ρ, m_{t} and J_{t} are the effective mass density of the Fe-Ga beam with a coil, the mass of the tip mass, and the moment of inertia of the tip mass, respectively. l and l_{t} are the length of the double-beam and the length of the tip mass, respectively. The strain energy density u and magnetic energy density u_{m} are defined as follows:

$$\begin{aligned}u &= \frac{1}{2}\Delta T\Delta S \\ &= \frac{1}{2}\frac{z^2}{z_0}\frac{\nu^{\mathrm{T}}E^{\mathrm{H}}d}{1-k_0^2}\frac{\partial^2\psi_{(x)}}{\partial x^2}\eta B_{\mathrm{ave}} + \frac{1}{2}z^2\frac{E^{\mathrm{H}}}{1-k_0^2}\left(\frac{\partial^2\psi_{(x)}}{\partial x^2}\right)^2\eta^2 = \frac{1}{2}\frac{z^2}{z_0 A}\frac{\nu^{\mathrm{T}}E^{\mathrm{H}}d}{1-k_0^2}\frac{\partial^2\psi_{(x)}}{\partial x^2}\eta\phi + \frac{1}{2}z^2\frac{E^{\mathrm{H}}}{1-k_0^2}\left(\frac{\partial^2\psi_{(x)}}{\partial x^2}\right)^2\eta^2 \\ u_{\mathrm{m}} &= \frac{1}{2}\Delta H\Delta B \\ &= \frac{1}{2}\frac{z^2}{z_0}\frac{\nu^{\mathrm{T}}E^{\mathrm{H}}d}{1-k_0^2}\frac{\partial^2\psi_{(x)}}{\partial x^2}\eta B_{\mathrm{ave}} + \frac{1}{2}\frac{z^2}{z_0^2}\frac{\nu^{\mathrm{T}}}{1-k_0^2}B_{\mathrm{ave}}^2 = \frac{1}{2}\frac{z^2}{z_0 A}\frac{\nu^{\mathrm{T}}E^{\mathrm{H}}d}{1-k_0^2}\frac{\partial^2\psi_{(x)}}{\partial x^2}\eta\phi + \frac{1}{2}\frac{z^2}{z_0^2A^2}\frac{\nu^{\mathrm{T}}}{1-k_0^2}\phi^2\end{aligned} \tag{24}$$

where Eqs. (3), (6) and (7) are used. When system configuration is assumed to be known at t_a and t_b ($\delta\eta_{(t_a)} \equiv \delta\eta_{(t_b)} \equiv \delta\phi_{(t_a)} \equiv \delta\phi_{(t_b)} \equiv \delta q_{(t_a)} \equiv \delta q_{(t_b)} \equiv 0$), Eq. (21) is called Hamilton's principle and this principle is often used to derive equations of systems [27,28].

However, the system configuration does not have to be known. This fact can be confirmed by applying Taylor expansion to $\delta\mathcal{L}$ in Eq. (21):

$$\int_{t_a}^{t_b}\left(\frac{\partial\mathcal{L}}{\partial\eta}\delta\eta+\frac{\partial\mathcal{L}}{\partial\phi}\delta\phi+\frac{\partial\mathcal{L}}{\partial q}\delta q\right)\mathrm{d}t+\int_{t_a}^{t_b}\left(\frac{\partial\mathcal{L}}{\partial\dot{\eta}}\delta\dot{\eta}+\frac{\partial\mathcal{L}}{\partial\dot{\phi}}\delta\dot{\phi}+\frac{\partial\mathcal{L}}{\partial\dot{q}}\delta\dot{q}\right)\mathrm{d}t-\left[m\dot{\eta}\delta\eta+L\dot{q}\delta q+N\dot{\phi}\delta q\right]_{t_a}^{t_b}=0 \tag{25}$$

where the second term of Eq. (25) can be represented by the integration by parts as

$$\int_{t_a}^{t_b}\left(\frac{\partial\mathcal{L}}{\partial\dot{\eta}}\delta\dot{\eta}+\frac{\partial\mathcal{L}}{\partial\dot{\phi}}\delta\dot{\phi}+\frac{\partial\mathcal{L}}{\partial\dot{q}}\delta\dot{q}\right)\mathrm{d}t=\left[m\dot{\eta}\delta\eta+L\dot{q}\delta q+N\dot{\phi}\delta q\right]_{t_a}^{t_b}-\int_{t_a}^{t_b}\left[\frac{\mathrm{d}}{\mathrm{d}t}\left(\frac{\partial\mathcal{L}}{\partial\dot{\eta}}\right)\delta\eta+\frac{\mathrm{d}}{\mathrm{d}t}\left(\frac{\partial\mathcal{L}}{\partial\dot{\phi}}\delta\dot{\phi}\right)+\frac{\mathrm{d}}{\mathrm{d}t}\left(\frac{\partial\mathcal{L}}{\partial\dot{q}}\delta\dot{q}\right)\right]\mathrm{d}t \tag{26}$$

Therefore, Eq. (25) becomes

$$\int_{t_a}^{t_b}\left\{\left[\frac{\partial\mathcal{L}}{\partial\eta}-\frac{\mathrm{d}}{\mathrm{d}t}\left(\frac{\partial\mathcal{L}}{\partial\dot{\eta}}\right)\right]\delta\eta+\left[\frac{\partial\mathcal{L}}{\partial\phi}-\frac{\mathrm{d}}{\mathrm{d}t}\left(\frac{\partial\mathcal{L}}{\partial\dot{\phi}}\right)\right]\delta\phi+\left[\frac{\partial\mathcal{L}}{\partial q}-\frac{\mathrm{d}}{\mathrm{d}t}\left(\frac{\partial\mathcal{L}}{\partial\dot{q}}\right)\right]\delta q\right\}\mathrm{d}t=0 \tag{27}$$

Because t_a and t_b are arbitrary, the integrand of Eq. (27) has to be zero:

$$\left[\frac{\partial\mathcal{L}}{\partial\eta}-\frac{\mathrm{d}}{\mathrm{d}t}\left(\frac{\partial\mathcal{L}}{\partial\dot{\eta}}\right)\right]\delta\eta+\left[\frac{\partial\mathcal{L}}{\partial\phi}-\frac{\mathrm{d}}{\mathrm{d}t}\left(\frac{\partial\mathcal{L}}{\partial\dot{\phi}}\right)\right]\delta\phi+\left[\frac{\partial\mathcal{L}}{\partial q}-\frac{\mathrm{d}}{\mathrm{d}t}\left(\frac{\partial\mathcal{L}}{\partial\dot{q}}\right)\right]\delta q=0 \tag{28}$$

Eq. (28) also represents the total virtual work Eq. (19). The infinitesimally small virtual quantities $\delta\eta$, $\delta\phi$, and δq are also arbitrary, and thus Eq. (28) has to be an identical equation with respect to the virtual quantities:

$$\begin{aligned}
&\frac{\mathrm{d}}{\mathrm{d}t}\left(\frac{\partial\mathcal{L}}{\partial\dot{\eta}}\right)-\frac{\partial\mathcal{L}}{\partial\eta}=0\\
&\frac{\mathrm{d}}{\mathrm{d}t}\left(\frac{\partial\mathcal{L}}{\partial\dot{\phi}}\right)-\frac{\partial\mathcal{L}}{\partial\phi}=0\\
&\frac{\mathrm{d}}{\mathrm{d}t}\left(\frac{\partial\mathcal{L}}{\partial\dot{q}}\right)-\frac{\partial\mathcal{L}}{\partial q}=0
\end{aligned} \tag{29}$$

Eqs. (29) are Euler–Lagrange equations for an electromagnetic-mechanically coupled conserved system. These equations show that D'Alembert's law and Kirchhoff's second law in the electric and magnetic circuits can be described by the energies of the system, which can be confirmed by comparing Eqs. (19) and (28). To expand Eqs. (29) for a non-conserved system, a damping term is added as follows:

$$\begin{aligned}
&\frac{\mathrm{d}}{\mathrm{d}t}\left(\frac{\partial\mathcal{L}}{\partial\dot{\eta}}\right)-\frac{\partial\mathcal{L}}{\partial\eta}+\frac{\partial D}{\partial\dot{\eta}}=m\ddot{\eta}+c\dot{\eta}+k\eta+\theta\phi=0\\
&\frac{\mathrm{d}}{\mathrm{d}t}\left(\frac{\partial\mathcal{L}}{\partial\dot{\phi}}\right)-\frac{\partial\mathcal{L}}{\partial\phi}+\frac{\partial D}{\partial\dot{\phi}}=\theta\phi+\mathcal{R}\phi-N\dot{q}=0\\
&\frac{\mathrm{d}}{\mathrm{d}t}\left(\frac{\partial\mathcal{L}}{\partial\dot{q}}\right)-\frac{\partial\mathcal{L}}{\partial q}+\frac{\partial D}{\partial\dot{q}}=N\dot{\phi}+\left(R_{\mathrm{coil}}+R\right)\dot{q}=0
\end{aligned} \tag{30}$$

with the following parameters:

$$\begin{aligned}
&\text{Generalized mass: } m=2\int_0^l\rho A\psi_{(x)}^2\mathrm{d}x+m_{\mathrm{t}}\left(\psi_{(l)}+\frac{1}{2}\left.\frac{\partial\psi_{(x)}}{\partial x}\right|_{x=l}l_{\mathrm{t}}\right)^2+J_{\mathrm{t}}\left(\left.\frac{\partial\psi_{(x)}}{\partial x}\right|_{x=l}\right)^2\\
&\text{Generalized spring constant: } k=2\int_0^l\int_A z^2\frac{E^{\mathrm{H}}}{1-k_0^2}\left(\frac{\partial^2\psi_{(x)}}{\partial x^2}\right)^2\mathrm{d}A\mathrm{d}x\\
&\text{Magneto-mechanical coupling coefficient: } \theta=2\int_0^l\int_A\frac{z^2}{z_0A}\frac{\nu^{\mathrm{T}}E^{\mathrm{H}}d}{1-k_0^2}\frac{\partial^2\psi_{(x)}}{\partial x^2}\mathrm{d}A\mathrm{d}x\\
&\text{Generalized magnetic resistance: } \mathcal{R}=2\int_0^l\int_A\frac{z^2}{z_0^2A^2}\frac{\nu^{\mathrm{T}}}{1-k_0^2}\mathrm{d}A\mathrm{d}x
\end{aligned} \tag{31}$$

where D is called Rayleigh's dissipation function. In this study, the vibrational energy is dissipated by primary damping, the resistance of coil R_{coil}, and load resistance R of the electric circuit. In such case, D is defined as follows:

$$D=\frac{1}{2}c\dot{\eta}^2+\frac{1}{2}R_{\mathrm{coil}}\dot{q}^2+\frac{1}{2}R\dot{q}^2 \tag{32}$$

where c is the primary damping coefficient. The primary damping represents the uncertain damping due to air resistance, mechanical hysteresis [29], magnetic hysteresis [30], and eddy current effect [20] acting on the cantilever. For energy harvesting, given mechanical energy needs to be dissipated by a load which is for the sake of this analysis represented as a simple resistor.

In Eqs. (30), it is evident that the double-beam cantilever is converted into a single-degree-of-freedom spring–mass–damper system, and each equation corresponds to a general equation of motion, a general magnetic circuit equation, and an electric circuit equation, respectively. This means that Eqs. (30) are the generalized system of equations for a single-degree-of-freedom electromagnetic-mechanical coupled system.

3. Harvestable energy from impact vibration

In this section, we derive the energy dissipated in the load resistance. The dissipated energy can be considered as harvestable energy [12]. When we consider the free vibration induced by impact energy, Eqs. (30) can be represented as a matrix equation as

$$\begin{bmatrix} m\lambda^2 + c\lambda + k & \theta & 0 \\ \theta & \mathcal{R} & -N \\ 0 & N\lambda & R_{\mathrm{coil}} + R \end{bmatrix} \begin{bmatrix} \eta \\ \phi \\ \dot{q} \end{bmatrix} = \mathbf{0} \tag{33}$$

where λ is the complex eigenvalue. The complex eigenvalues can be obtained by solving the following characteristic equation:

$$\det \begin{bmatrix} m\lambda^2 + c\lambda + k & \theta & 0 \\ \theta & \mathcal{R} & -N \\ 0 & N\lambda & R_{\mathrm{coil}} + R \end{bmatrix} = a_0\lambda^3 + a_1\lambda^2 + a_2\lambda + a_3 = 0 \tag{34}$$

where

$$\begin{aligned} a_0 &= N^2\, m \\ a_1 &= N^2 c + R\mathcal{R}m + R_{\mathrm{coil}}\mathcal{R}m \\ a_2 &= N^2 k + R\mathcal{R}c + R_{\mathrm{coil}}\mathcal{R}c \\ a_3 &= R\mathcal{R}k - R\theta^2 + R_{\mathrm{coil}}\mathcal{R}k - R_{\mathrm{coil}}\theta^2 \end{aligned} \tag{35}$$

Using the complex eigenvalues λ_1, λ_2 and λ_3, the non-trivial solution $\dot{q}$ of Eq. (33) can be represented as follows:

$$\dot{q} = X_1 e^{\lambda_1 t} + X_2 e^{\lambda_2 t} + X_3 e^{\lambda_3 t} \tag{36}$$

where the coefficients X_1, X_2 and X_3 are determined by the initial value of the generalized displacement $\eta_{(0)}$, generalized velocity $\dot{\eta}_{(0)}$ and current $\dot{q}_{(0)}$. In this study, we considered no initial current $\left(\dot{q}_{(0)} = 0\right)$. In this case, X_1, X_2 and X_3 are respectively given as follows:

$$\begin{aligned} X_1 &= \frac{N\theta\lambda_1\lambda_2\lambda_3}{\mathcal{R}\left(R_{\mathrm{coil}} + R\right)\left(\lambda_1 - \lambda_2\right)\left(\lambda_1 - \lambda_3\right)}\eta_{(0)} + \frac{\theta\lambda_1}{N\left(\lambda_1 - \lambda_2\right)\left(\lambda_1 - \lambda_3\right)}\dot{\eta}_{(0)} \\ X_2 &= \frac{N\theta\lambda_1\lambda_2\lambda_3}{\mathcal{R}\left(R_{\mathrm{coil}} + R\right)\left(\lambda_2 - \lambda_1\right)\left(\lambda_2 - \lambda_3\right)}\eta_{(0)} + \frac{\theta\lambda_2}{N\left(\lambda_2 - \lambda_1\right)\left(\lambda_2 - \lambda_3\right)}\dot{\eta}_{(0)} \\ X_3 &= \frac{N\theta\lambda_1\lambda_2\lambda_3}{\mathcal{R}\left(R_{\mathrm{coil}} + R\right)\left(\lambda_3 - \lambda_2\right)\left(\lambda_3 - \lambda_1\right)}\eta_{(0)} + \frac{\theta\lambda_3}{N\left(\lambda_3 - \lambda_2\right)\left(\lambda_3 - \lambda_1\right)}\dot{\eta}_{(0)} \end{aligned} \tag{37}$$

The harvestable energy Q from the electric circuit can be obtained by integrating the output power P over infinite time:

$$Q = \int_0^\infty P\mathrm{d}t = \int_0^\infty \dot{q}^2 R\mathrm{d}t = -\frac{RN^2\theta^2}{2\mathcal{R}^2\left(R_{\mathrm{coil}} + R\right)^2}\frac{\mathrm{Num}}{\mathrm{Den}}\eta_{(0)}^2 - \frac{R\theta^2}{2N^2}\frac{1}{\mathrm{Den}}\dot{\eta}_{(0)}^2 \tag{38}$$

where

$$\begin{aligned} \mathrm{Den} &= \left(\lambda_1 + \lambda_2\right)\left(\lambda_2 + \lambda_3\right)\left(\lambda_3 + \lambda_1\right) \\ \mathrm{Num} &= \lambda_1\lambda_2\lambda_3\left(\lambda_1 + \lambda_2 + \lambda_3\right) \end{aligned} \tag{39}$$

Eq. (38) is a symmetric expression with regards to the complex eigenvalues λ_1, λ_2 and λ_3, and thus it can be represented as

$$Q = -\frac{RN^2\theta^2}{2\mathcal{R}^2\left(R_{\mathrm{coil}} + R\right)^2}\frac{b_1 b_3}{b_1 b_2 - b_3}\eta_{(0)}^2 - \frac{R\theta^2}{2N^2}\frac{1}{b_1 b_2 - b_3}\dot{\eta}_{(0)}^2 \tag{40}$$

where b_1, b_2 and b_3 are the elementary symmetric polynomials:

$$\begin{aligned} b_1 &= \lambda_1 + \lambda_2 + \lambda_3 \\ b_2 &= \lambda_1\lambda_2 + \lambda_1\lambda_3 + \lambda_2\lambda_3 \\ b_3 &= \lambda_1\lambda_2\lambda_3 \end{aligned} \tag{41}$$

Eqs. (41) can be linked with Eqs. (35) by the Vieta's formulas:

$$\begin{aligned} b_1 &= -\frac{a_1}{a_0} \\ b_2 &= \frac{a_2}{a_0} \\ b_3 &= -\frac{a_3}{a_0} \end{aligned} \tag{42}$$

From Eqs. (35), (40) and (42), the harvestable energy Q can finally be obtained as

$$\begin{aligned} Q =& \frac{1}{2}\left(k-\frac{\theta^2}{\mathcal{R}}\right)\frac{\left(\alpha\zeta_2+\zeta_1+\zeta_2\right)\alpha\kappa}{\left(4\alpha^2\zeta_1\zeta_2^2+4\alpha\zeta_1^2\zeta_2+8\alpha\zeta_1\zeta_2^2+\alpha\kappa\zeta_2+4\zeta_1^2\zeta_2+4\zeta_1\zeta_2^2+\kappa\zeta_1+\kappa\zeta_2+\zeta_1\right)(\alpha+1)}\eta_{(0)}^2 \\ &+ \frac{1}{2}m\frac{\alpha\kappa\zeta_2}{4\alpha^2\zeta_1\zeta_2^2+4\alpha\zeta_1^2\zeta_2+8\alpha\zeta_1\zeta_2^2+\alpha\kappa\zeta_2+4\zeta_1^2\zeta_2+4\zeta_1\zeta_2^2+\kappa\zeta_1+\kappa\zeta_2+\zeta_1}\dot{\eta}_{(0)}^2 \end{aligned} \tag{43}$$

where each non-dimensional parameter is defined as follows:

$$\begin{aligned} &\text{Magnetostrictive coupling constant: } \kappa = \frac{\theta^2}{k\mathcal{R}-\theta^2} \\ &\text{Primary damping ratio: } \zeta_1 = \frac{c}{2\,m\omega} \\ &\text{Damping ratio of coil resistance: } \zeta_2 = \frac{R_{\text{coil}}}{2\left(\frac{N^2}{\mathcal{R}}\right)\omega} \\ &\text{Resistance ratio between coil and load resistance } \alpha = \frac{R}{R_{\text{coil}}} \end{aligned} \tag{44}$$

where ω is the undamped natural frequency of the mechanical-magnetic system:

$$\omega = \sqrt{\frac{k-\frac{\theta^2}{\mathcal{R}}}{m}} \tag{45}$$

It is noteworthy that when the system has no primary damping and no coil resistance, Eq. (43) becomes

$$Q_{\text{in}} = \frac{1}{2}\left(k-\frac{\theta^2}{\mathcal{R}}\right)\eta_{(0)}^2 + \frac{1}{2}m\dot{\eta}_{(0)}^2 \tag{46}$$

Eq. (46) exactly represents the initially given mechanical energy. This means that all given mechanical energy is dissipated by the resistance in the electric circuit when other damping elements do not exist.

4. Efficiency maximization

In many practical applications [21,31,32], free vibration is induced by either initial displacement or initial velocity, but not both. In this study, we maximize the energy harvesting efficiency E to given potential energy (denoted by subscript U) and given kinetic energy (denoted by subscript K), respectively, and compare their optimal conditions. Each objective function E_U and E_K can be obtained from Eqs. (43) and (46) as follows:

$$\begin{aligned} E_U &= \left.\frac{Q}{Q_{\text{in}}}\right|_{\dot{\eta}_{(0)}=0} = \frac{\left(\alpha\zeta_2+\zeta_1+\zeta_2\right)\alpha\kappa}{\left(4\alpha^2\zeta_1\zeta_2^2+4\alpha\zeta_1^2\zeta_2+8\alpha\zeta_1\zeta_2^2+\alpha\kappa\zeta_2+4\zeta_1^2\zeta_2+4\zeta_1\zeta_2^2+\kappa\zeta_1+\kappa\zeta_2+\zeta_1\right)(\alpha+1)} \\ E_K &= \left.\frac{Q}{Q_{\text{in}}}\right|_{\eta_{(0)}=0} = \frac{\alpha\kappa\zeta_2}{4\alpha^2\zeta_1\zeta_2^2+4\alpha\zeta_1^2\zeta_2+8\alpha\zeta_1\zeta_2^2+\alpha\kappa\zeta_2+4\zeta_1^2\zeta_2+4\zeta_1\zeta_2^2+\kappa\zeta_1+\kappa\zeta_2+\zeta_1} \end{aligned} \tag{47}$$

The energy harvesting efficiencies Eqs. (47) can completely be represented with four non-dimensional design parameters Eq. (44), and respectively have a global maximum with respect to α. With given optimal resistance ratio α_{opt}, they become increasing functions with respect to κ, and decreasing functions with respect to ζ_1 and ζ_2. The optimal resistance ratio α_{opt} at which the harvestable energy is maximized can be obtained by solving the following equation:

$$\frac{\partial E}{\partial \alpha} = 0 \tag{48}$$

4.1. Efficiency to potential energy

For the efficiency maximization to initial potential energy, the optimal condition Eq. (48) is represented as follows:

$$\begin{aligned} &4\zeta_1\zeta_2^3\alpha_{\text{opt}}^4 + \left(8\zeta_1^2\zeta_2^2+8\zeta_1\zeta_2^3\right)\alpha_{\text{opt}}^3 + \left(4\zeta_1^3\zeta_2+8\zeta_1^2\zeta_2^2-\kappa\zeta_2^2-\zeta_1\zeta_2\right)\alpha_{\text{opt}}^2 \\ &+ \left(-8\zeta_1^2\zeta_2^2-8\zeta_1\zeta_2^3-2\kappa\zeta_1\zeta_2-2\kappa\zeta_2^2-2\zeta_1\zeta_2\right)\alpha_{\text{opt}} \\ &- 4\zeta_1^3\zeta_2-8\zeta_1^2\zeta_2^2-4\zeta_1\zeta_2^3-\kappa\zeta_1^2-2\kappa\zeta_1\zeta_2-\kappa\zeta_2^2-\zeta_1^2-\zeta_1\zeta_2 = 0 \end{aligned} \tag{49}$$

Eq. (49) can be solved algebraically by Ferrari's method:

$$\alpha_{\text{opt}} = \frac{1}{2}\left(\sqrt{2\Lambda-p_1}+\sqrt{-2\Lambda-p_1-\frac{2p_2}{\sqrt{2\Lambda-p_1}}}-\frac{\zeta_1+\zeta_2}{\zeta_2}\right) \tag{50}$$

where

$$\Lambda = \frac{p_1}{6}+r-\frac{w_1}{3r} \tag{51}$$

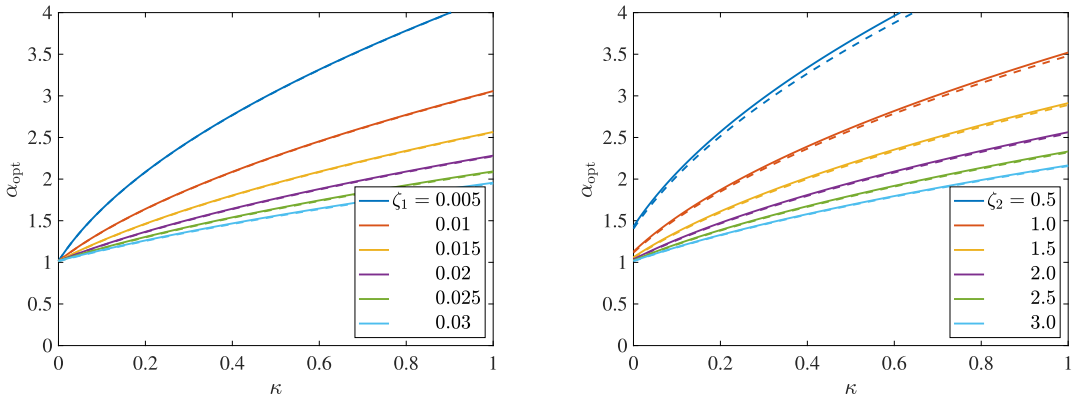

(a) Variation of the primary damping ratio ζ_1 ($\zeta_2 = 3.016$) (b) Variation of the coil resistance damping ratio ζ_2 ($\zeta_1 = 0.023$)

Fig. 4. Optimal resistance ratio α_{opt} to maximize efficiency to kinetic energy (solid line) and potential energy (dashed line).

$$r = \sqrt[3]{-\frac{w_2}{2} + \sqrt{\frac{w_2^2}{4} + \frac{w_1^3}{27}}} \tag{52}$$

$$\begin{aligned} w_1 &= -\frac{p_1^2}{12} - p_3 \\ w_2 &= -\frac{p_1^3}{108} + \frac{p_1 p_3}{3} - \frac{p_2^2}{8} \end{aligned} \tag{53}$$

$$\begin{aligned} p_1 &= -\frac{1}{4\zeta_1\zeta_2^2}\left(2\zeta_1^3 + 4\zeta_1^2\zeta_2 + 6\zeta_1\zeta_2^2 + \kappa\zeta_2 + \zeta_1\right) \\ p_2 &= -\frac{1}{4\zeta_1\zeta_2^3}\left(4\zeta_1^2\zeta_2^2 + 4\zeta_1\zeta_2^3 + \kappa\zeta_1\zeta_2 + \kappa\zeta_2^2 - \zeta_1^2 + \zeta_1\zeta_2\right) \\ p_3 &= \frac{1}{16\zeta_1\zeta_2^4}\left(\zeta_1^5 + 4\zeta_1^4\zeta_2 + 2\zeta_1^3\zeta_2^2 - 4\zeta_1^2\zeta_2^3 - 3\zeta_1\zeta_2^4 - \kappa\zeta_1^2\zeta_2 - 2\kappa\zeta_1\zeta_2^2 - \kappa\zeta_2^3 - \zeta_1^3 - 2\zeta_1^2\zeta_2 - \zeta_1\zeta_2^2\right) \end{aligned} \tag{54}$$

4.2. Efficiency to kinetic energy

For the efficiency to the kinetic energy E_K, Eq. (48) can be represented as follows:

$$4\zeta_1\zeta_2^2\alpha_{\mathrm{opt}}^2 - 4\zeta_1^2\zeta_2 - 4\zeta_1\zeta_2^2 - \kappa\zeta_1 - \kappa\zeta_2 - \zeta_1 = 0 \tag{55}$$

Eq. (55) can also be solved algebraically, which yields

$$\alpha_{\mathrm{opt}} = \frac{\sqrt{\zeta_1\left(4\zeta_1^2\zeta_2 + 4\zeta_1\zeta_2^2 + \kappa\zeta_1 + \kappa\zeta_2 + \zeta_1\right)}}{2\zeta_1\zeta_2} \tag{56}$$

Figs. 4 and 5 respectively show the optimal resistance ratio α_{opt} and maximized efficiencies $E_{K\max}$ and $E_{U\max}$ with different (a) ζ_1 and (b) ζ_2. Even though Eq. (56) is much simpler than Eq. (50), Eq. (56) is approximately equal to Eq. (50) in a wide range of the parameters as shown in Figs. 4. Thus, when the harvestable kinetic energy is maximized, also the harvestable potential energy is nearly maximized, and vice versa.

5. Experiments

Fig. 6 shows the double-beam magnetostrictive energy harvester for experiments. The two Fe-Ga beams were attached to an aluminum beam by superglue. In the double-beam section, copper coils with 0.2 mm diameter were wound around each Fe-Ga beam and they were connected in series so that the voltages in the coils are induced in the same direction. In this study, we assumed that the tip mass is stiff enough to be treated as a rigid body.

Table 1 lists the values of the parameters measured for the analytical calculation. The effective mass density ρ was measured from the weight of the Fe-Ga beam and the copper coil. The Young's modulus E^{H} was calculated from the natural frequency of the single Fe-Ga beam measured by the free vibration experiment. Fig. 7(a) shows its experimental setup. The tip of the single Fe-Ga beam was plucked to induce free vibration. The free vibration response was measured by a laser displacement sensor (optoNCDT

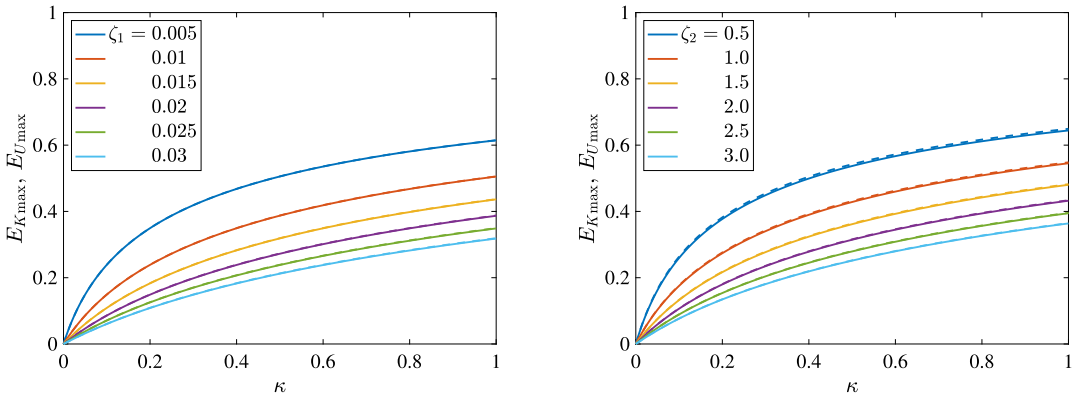

(a) Variation of the primary damping ratio ζ_1 ($\zeta_2 = 3.016$) (b) Variation of the coil resistance damping ratio ζ_2 ($\zeta_1 = 0.023$)

Fig. 5. Maximized efficiencies $E_{K\max}$ (solid line) and $E_{U\max}$ (dashed line).

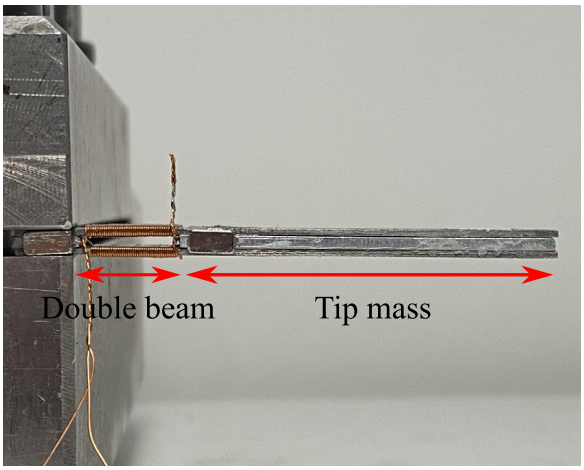

Fig. 6. Double-beam magnetostrictive energy harvester for experiments.

Table 1
Values of parameters of experimental magnetostrictive energy harvester.

Parameter	Definition	Value
ρ	Effective mass density of Fe-Ga beam with coil	1.46×10^4 kg m^{-3}
b	Width of Fe-Ga beam	5.92×10^{-3} m
h	Height of Fe-Ga beam	7.20×10^{-4} m
z_0	Central coordinate of upper Fe-Ga beam	1.11×10^{-3} m
l	Double-beam length	1.10×10^{-2} m
l_t	Tip mass length	4.21×10^{-2} m
m_t	Tip mass weight	5.85×10^{-3} kg
J_t	Moment of inertia of tip mass	3.46×10^{-6} kg m^2
ν^T	Magnetic reluctivity of Fe-Ga	10000 m H^{-1}
E^H	Young's modulus of Fe-Ga	52.1 GPa
d	Magnetostrictive constant of Fe-Ga	5.0 nm A^{-1}
N	Total number of turns in coils	80
R_{coil}	Resistance of coil	1.80 Ω
ζ_1	Primary damping ratio of harvester	0.023

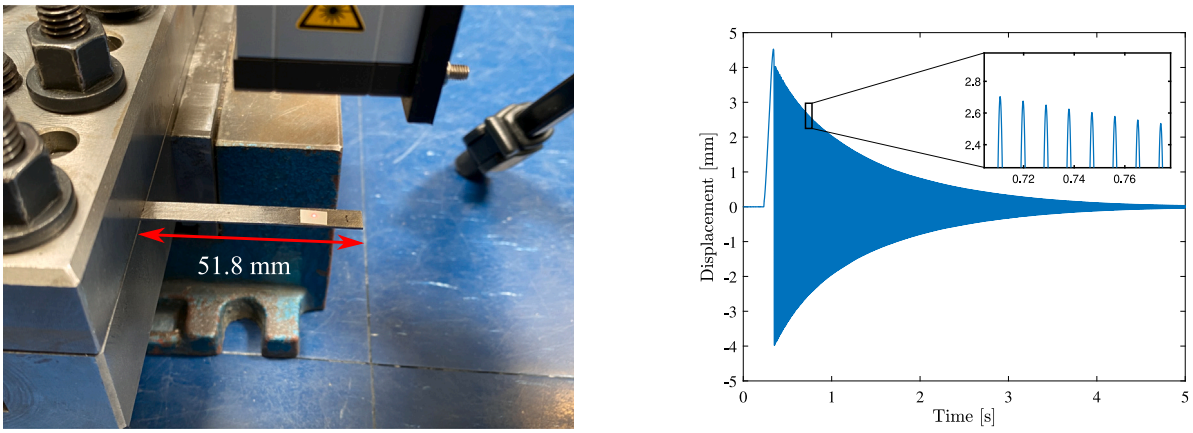

(a) Experimental setup (b) Free vibration response of single Fe-Ga beam

Fig. 7. Free vibration experiment of single Fe-Ga beam for measuring Young's modulus E^{H} of Fe-Ga.

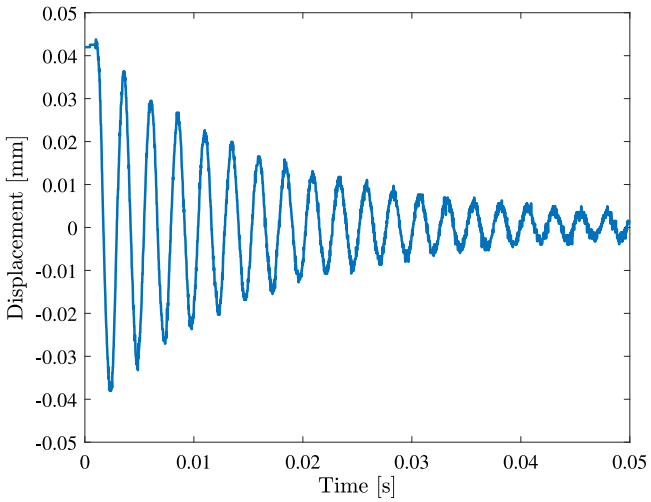

Fig. 8. Free vibration response of the open-circuited magnetostrictive energy harvester.

1900 from Micro-Epsilon). The natural frequency of 109.9 Hz was obtained from the free vibration response shown in Fig. 7(b). In this experiment, we assumed that the Fe-Ga beam oscillated with only its fundamental mode of oscillation. The free vibration response of the magnetostrictive energy harvester with an open circuit was also measured to determine the primary damping ratio ζ_1. From the obtained free vibration response with a 300 g weight (Fig. 8), ζ_1 was calculated by the logarithmic decrement method. The magnetostrictive constant d was determined from the voltage responses of the harvester with $R = 10.0\ \Omega$ ($\alpha = 5.56$). Fig. 9 shows the schematic view of the experimental setup. The initial displacements $\psi_{(l)}\eta_{(0)} = -14.5$, -27.1, and -43.1 μm were given at the end of the double beam by hanging 100 g, 200 g, and 300 g weights, respectively, at the tip of the harvester via string. The subsequent free vibration was then induced by cutting the string. As shown in Figs. 10 (a)–(c), a value of $d = 5.0$ nm A^{-1} was observed to give a good match between the calculated and the measured voltage responses, which proves the linearity of the harvested energy with respect to the initial displacement.

The initial displacement tests were repeated for different resistance ratios α for validating the efficiency calculations. The resistance ratio was varied by tuning the load resistance R. The harvested energy was calculated from the measured load voltage V as

$$Q = \int_0^{\infty} P\mathrm{d}t \approx \int_0^{\tau} \frac{V^2}{R}\mathrm{d}t \tag{57}$$

The output power P was integrated for $\tau = 5$ seconds based on the assumption that the free vibration of the experimental device completely stops within this time. The energy harvesting efficiency E_U of the experimental device was calculated by dividing Q by Eq. (46). Fig. 11 shows the variation of the energy harvesting efficiency E_U with respect to the resistance ratio α. The theoretical

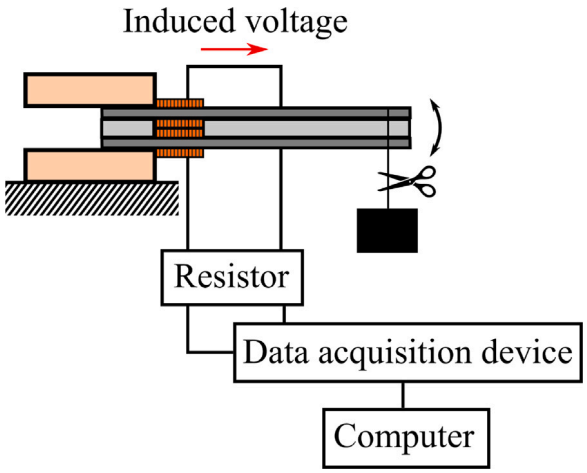

Fig. 9. Schematic view of experimental setup for measuring free voltage response.

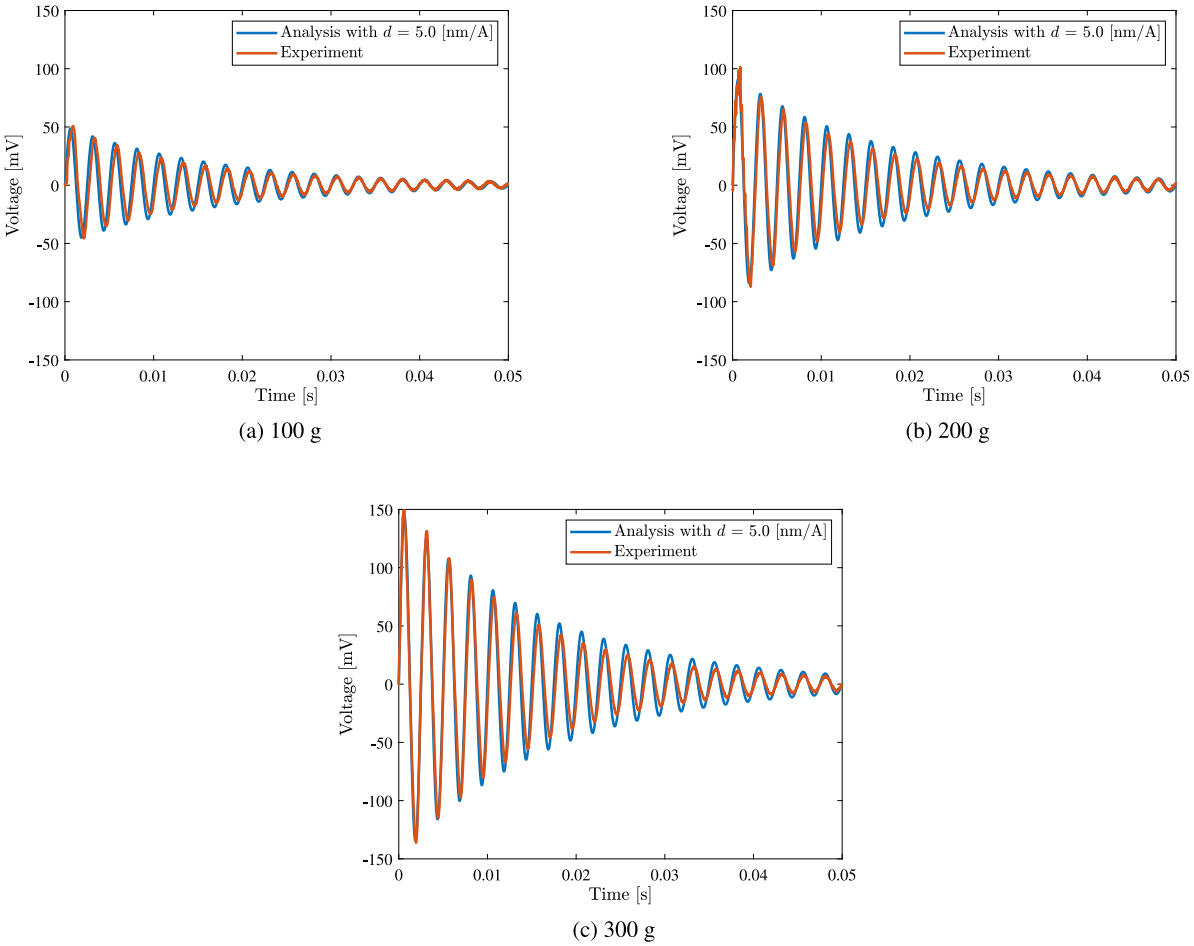

Fig. 10. Free voltage responses for determining magnetostrictive constant d.

optimal resistance ratio $\alpha_{\mathrm{opt}} = 1.037$ was calculated by Eq. (50) using the parameters in Table 1. The efficiencies and the efficiency-maximizing load resistance ratio in Fig. 11 agree well with the analytical results, and the validity of the proposed modeling method for the magnetostrictive energy harvester is confirmed.

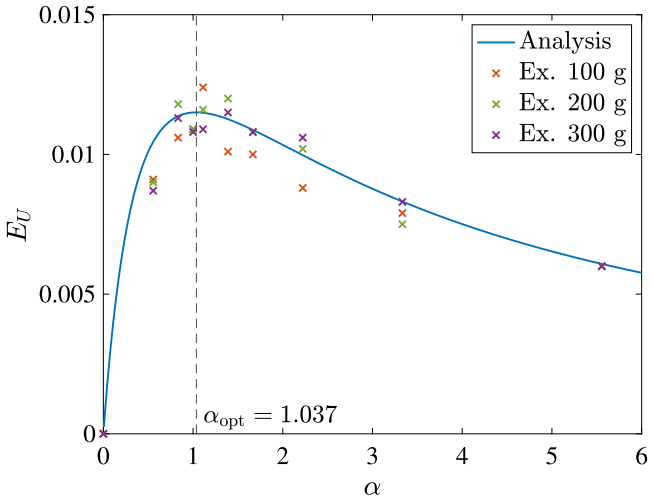

Fig. 11. Variation of energy harvesting efficiency E_U with respect to resistance ratio α.

6. Conclusion

This paper presented a modeling and optimization method of the magnetostrictive energy harvester based on energy harvesting efficiency for free vibration. In the modeling of the double-beam magnetostrictive energy harvester, the shape function was derived as a quadratic function based on the continuity of the internal force and magnetic flux. The calculation process presented in this paper is simpler compared to solving the frequency equation. The Euler–Lagrange equations for an electromagnetic-mechanically coupled system were derived based on D'Alembert's principle, Faraday's law, and Ampere's law. The harvestable energy of the magnetostrictive energy harvester was calculated by using the symmetric property of eigenvalues. In the experiments, Young's modulus, primary damping ratio, and magnetostrictive constant were determined by the free vibration responses for the analytical calculation. The proposed modeling method was validated by measuring the energy harvesting efficiency to given potential energy at different resistance ratios.

Based on the analytical calculation, the optimal resistance ratio to maximize the energy harvesting efficiency is found to be different depending on the type of given energy. The algebraically obtained optimal resistance ratio to maximize the harvestable kinetic energy is considerably simple compared to that of potential energy. However, this study has shown that they are approximately equal in a wide range, which means that the energy harvesting efficiency can nearly be maximized with the derived resistance ratio even when the harvester experiences free vibrations induced by a combination of initial displacement and velocity. The gap between these optimal resistance ratios becomes greater with the increase of the magnetostrictive coupling coefficient and the number of turns which are the important parameters to increase the energy harvesting efficiency. In such a case, the appropriate optimal resistance ratio should be chosen or modified depending on the application.

The method and optimal design parameters presented here can be used for a general magneto-mechanical coupled system with a resistive circuit, and easily extended to advance the development of potential-energy-optimized energy harvesters based on plucking or frequency up-conversion mechanisms with periodic controlled impact excitations [33,34].

CRediT authorship contribution statement

Yoshito Mizukawa: Conceptualization, Methodology, Formal analysis, Investigation, Writing – original draft, Funding acquisition. **Umair Ahmed:** Investigation, Writing – review & editing. **David Blažević:** Writing – review & editing, Supervision. **Paavo Rasilo:** Writing – review & editing, Supervision, Funding acquisition.

Declaration of competing interest

The authors declare that they have no known competing financial interests or personal relationships that could have appeared to influence the work reported in this paper.

Data availability

Data will be made available on request.

Acknowledgments

The author, Yoshito Mizukawa has received funding from the Aimo Puromäki special fund (No. 20200522) awarded by the KAUTE foundation, the Finnish Government Scholarship Pool (No. KM-20-11380) awarded by the Finnish National Agency for Education, and the Walter Ahlström Foundation (No. 20220102).

References

[1] S. Roundy, P.K. Wright, J.M. Rabaey, Energy Scavenging for Wireless Sensor Networks, Kluwer Academic Publishers, Boston, USA, 2003.
[2] T. Ueno, Magnetostrictive vibrational power generator for battery-free IoT application, AIP Adv. 9 (3) (2019) 035018, http://dx.doi.org/10.1063/1.5079882.
[3] J. Siang, M. Lim, M. Salman Leong, Review of vibration-based energy harvesting technology: Mechanism and architectural approach, Int. J. Energy Res. 42 (5) (2018) 1866–1893, http://dx.doi.org/10.1002/er.3986.
[4] S.R. Anton, D.J. Inman, Vibration energy harvesting for unmanned aerial vehicles, in: M. Ahmadian (Ed.), in: Active and Passive Smart Structures and Integrated Systems 2008, vol. 6928, SPIE, International Society for Optics and Photonics, 2008, p. 692824.
[5] X. Tang, L. Zuo, Simultaneous energy harvesting and vibration control of structures with tuned mass dampers, J. Intell. Mater. Syst. Struct. 23 (18) (2012) 2117–2127, http://dx.doi.org/10.1177/1045389X12462644.
[6] Y. Yoshida, Y. Kobayashi, T. Uchimura, Development of the monitoring system that operates with the power generated from the bridge vibration, J. Japan Soc. Civ. Eng., Ser. A1 (Structural Engineering & Earthquake Engineering (SE/EE)) 70 (2) (2014) 282–294, http://dx.doi.org/10.2208/jscejseee.70.282, (in Japanese).
[7] S.P. Beeby, R.N. Torah, M.J. Tudor, P. Glynne-Jones, T. O'Donnell, C.R. Saha, S. Roy, A micro electromagnetic generator for vibration energy harvesting, J. Micromech. Microeng. 17 (7) (2007) 1257–1265, http://dx.doi.org/10.1088/0960-1317/17/7/007.
[8] M.K. Abohamer, J. Awrejcewicz, R. Starosta, T.S. Amer, M.A. Bek, Influence of the motion of a spring pendulum on energy-harvesting devices, Appl. Sci. 11 (18) (2021) http://dx.doi.org/10.3390/app11188658.
[9] M.K. Abohamer, J. Awrejcewicz, T. Amer, Modeling of the vibration and stability of a dynamical system coupled with an energy harvesting device, Alex. Eng. J. 63 (2023) 377–397, http://dx.doi.org/10.1016/j.aej.2022.08.008.
[10] L. Zuo, W. Cui, Dual-functional energy-harvesting and vibration control: Electromagnetic resonant shunt series tuned mass dampers, J. Vib. Acoust. 135 (5) (2013) 051018, http://dx.doi.org/10.1115/1.4024095.
[11] A. Erturk, D.J. Inman, Mechanical considerations for modeling of vibration-based energy harvesters, in: Proceedings of the ASME 2007 International Design Engineering Technical Conferences and Computers and Information in Engineering Conference, 2007, pp. 769–778, http://dx.doi.org/10.1115/DETC2007-35440.
[12] E. Lefeuvre, D. Audigier, C. Richard, D. Guyomar, Buck-boost converter for sensorless power optimization of piezoelectric energy harvester, IEEE Trans. Power Electron. 22 (5) (2007) 2018–2025, http://dx.doi.org/10.1109/TPEL.2007.904230.
[13] P.V. Avvari, Y. Yang, C.K. Soh, Long-term fatigue behavior of a cantilever piezoelectric energy harvester, J. Intell. Mater. Syst. Struct. 28 (9) (2017) 1188–1210, http://dx.doi.org/10.1177/1045389X16667552.
[14] P.K. Panda, Review: Environmental friendly lead-free piezoelectric materials, J. Mater. Sci. 44 (19) (2009) 5049–5062, http://dx.doi.org/10.1007/s10853-009-3643-0.
[15] M. Safaei, H.A. Sodano, S.R. Anton, A review of energy harvesting using piezoelectric materials: State-of-the-art a decade later (2008–2018), Smart Mater. Struct. 28 (11) (2019) 113001, http://dx.doi.org/10.1088/1361-665x/ab36e4.
[16] S. Palumbo, P. Rasilo, M. Zucca, Experimental investigation on a Fe-Ga close yoke vibrational harvester by matching magnetic and mechanical biases, J. Magn. Magn. Mater. 469 (2019) 354–363, http://dx.doi.org/10.1016/j.jmmm.2018.08.085.
[17] U. Ahmed, J. Jeronen, M. Zucca, S. Palumbo, P. Rasilo, Finite element analysis of magnetostrictive energy harvesting concept device utilizing thermodynamic magneto-mechanical model, J. Magn. Magn. Mater. 486 (2019) 165275, http://dx.doi.org/10.1016/j.jmmm.2019.165275.
[18] U. Ahmed, U. Aydin, M. Zucca, S. Palumbo, R. Kouhia, P. Rasilo, Modeling a Fe-Ga energy harvester fitted with magnetic closure using 3D magneto-mechanical finite element model, J. Magn. Magn. Mater. 500 (2020) 166390, http://dx.doi.org/10.1016/j.jmmm.2020.166390.
[19] U. Ahmed, U. Aydin, L. Daniel, P. Rasilo, 3-D magneto-mechanical finite element analysis of galfenol-based energy harvester using an equivalent stress model, IEEE Trans. Magn. 57 (2) (2021) 1–5, http://dx.doi.org/10.1109/TMAG.2020.3011875.
[20] Y. Mizukawa, U. Ahmed, M. Zucca, D. Blažević, P. Rasilo, Small-signal modeling and optimal operating condition of magnetostrictive energy harvester, J. Magn. Magn. Mater. 547 (2022) 168819, http://dx.doi.org/10.1016/j.jmmm.2021.168819.
[21] T. Ueno, S. Yamada, Performance of energy harvester using iron–gallium alloy in free vibration, IEEE Trans. Magn. 47 (10) (2011) 2407–2409, http://dx.doi.org/10.1109/TMAG.2011.2158303.
[22] L. Wang, F.G. Yuan, Vibration energy harvesting by magnetostrictive material, Smart Mater. Struct. 17 (4) (2008) 045009, http://dx.doi.org/10.1088/0964-1726/17/4/045009.
[23] S. Timoshenko, Elements of Strength of Materials, fourth ed., repr., Van Nostrand, Princeton, NJ, 1964 - 1962.
[24] D. Davino, A. Giustiniani, C. Visone, A two-port nonlinear model for magnetoelastic energy-harvesting devices, IEEE Trans. Ind. Electron. 58 (6) (2011) 2556–2564, http://dx.doi.org/10.1109/TIE.2010.2062477.
[25] G. Engdahl, Handbook of Giant Magnetostrictive Materials, Academic Press, San Diego, CA, 2000.
[26] C.S. Clemente, A. Mahgoub, D. Davino, C. Visone, Multiphysics circuit of a magnetostrictive energy harvesting device, J. Intell. Mater. Syst. Struct. 28 (17) (2017) 2317–2330, http://dx.doi.org/10.1177/1045389X16685444.
[27] S.H. Crandall, Dynamics of Mechanical and Electromechanical Systems, McGraw-Hill, New York, 1968.
[28] A. Preumont, Mechatronics: Dynamics of Electromechanical and Piezoelectric Systems, Vol. 136, 2006.
[29] M. Bednarek, D. Lewandowski, K. Polczyński, J. Awrejcewicz, On the active damping of vibrations using electromagnetic spring, Mech. Based Des. Struct. Mach. 49 (8) (2021) 1131–1144, http://dx.doi.org/10.1080/15397734.2020.1819311.
[30] J.J. Scheidler, V.M. Asnani, M.J. Dapino, Frequency-dependent, dynamic sensing properties of polycrystalline Galfenol (Fe81.6Ga18.4), J. Appl. Phys. 119 (24) (2016) 244902, http://dx.doi.org/10.1063/1.4954320.
[31] S. Priya, Modeling of electric energy harvesting using piezoelectric windmill, Appl. Phys. Lett. 87 (18) (2005) 184101, http://dx.doi.org/10.1063/1.2119410.
[32] Y. Kuang, M. Zhu, Design study of a mechanically plucked piezoelectric energy harvester using validated finite element modelling, Sensors Actuators A 263 (2017) 510–520, http://dx.doi.org/10.1016/j.sna.2017.07.009.
[33] X. Li, G. Hu, Z. Guo, J. Wang, Y. Yang, J. Liang, Frequency up-conversion for vibration energy harvesting: A review, Symmetry 14 (3) (2022) 631, http://dx.doi.org/10.3390/sym14030631.
[34] M.M. Ahmad, N.M. Khan, F.U. Khan, Review of frequency up-conversion vibration energy harvesters using impact and plucking mechanism, Int. J. Energy Res. 45 (11) (2021) 15609–15645, http://dx.doi.org/10.1002/er.6832.